https://doi.org/10.2352/ISSN.2169-4451.2017.32.298

Reprinted from
Journal of Imaging Science and Technology® 60(4): 040402-1–040402-7, 2016.

Investigation on an Inkjet Printed Passive Sensor for Wireless Ice Detection on Wind Rotor Blades

M. Hartwig, M. Gaitzsch, and T. D. Großmann
Technische Universität Chemnitz, Reichenhainer Str. 70, 09126 Chemnitz, Germany
E-mail: melinda.hartwig@mb.tu-chemnitz.de

M. Heinrich
Fraunhofer-Institute for Machine Tools and Forming Technology (IWU), Reichenhainer Str. 88, 09123 Chemnitz, Germany

L. Kroll
Technische Universität Chemnitz, Reichenhainer Str. 70, 09126 Chemnitz, Germany
Fraunhofer-Institute for Machine Tools and Forming Technology (IWU), Reichenhainer Str. 88, 09123 Chemnitz Germany

T. Gessner
Technische Universität Chemnitz, Reichenhainer Str. 70, 09126 Chemnitz, Germany
Fraunhofer-Institute for Electronic Nano Systems (ENAS), Technologie-Campus 3, 09126 Chemnitz, Germany

R. R. Baumann▲
Technische Universität Chemnitz, Reichenhainer Str. 70, 09126 Chemnitz, Germany
Fraunhofer-Institute for Electronic Nano Systems (ENAS), Technologie-Campus 3, 09126 Chemnitz, Germany

Abstract. *Wireless reliability tests of lightweight composite materials by electromagnetic waves have become more and more interesting in the aerospace and automotive fields. The embedding of conductive printed patterns as electromagnetic resonators seems to be one of the useful techniques. The printing technology is a resource as well as time and cost efficient fabrication method to manufacture electronic devices. In particular, contactless and digital technologies like inkjet printing have great potential to be combined with integration processes like resin infusion technology. The combination of these manufacturing processes enables fast and efficient production of smart lightweight applications. The main focus of this work is the manufacture of a passive high frequency resonator on flexible substrates using inkjet printing. The conductive patterns are integrated into a composite material by resin infusion, enabling sensor applications in the field of clean energy, particularly for wireless ice detection on wind rotor blades.* © *2016 Society for Imaging Science and Technology.*

INTRODUCTION

Printing technologies like drop-on-demand inkjet printing lead to resource, cost and time efficient manufacturing. Using such a digital printing method, the patterns to be printed can be created very flexibly and no printing form is required. Moreover, expensive materials like silver ink can be applied efficiently as well as accurately with a small volume. As inkjet is a contactless printing method, various substrates can be chosen, especially flexible ones.[1–3] Printing technology enables low-cost, flexible and large-scale production of various electronic devices like thin-film transistors, radio-frequency identification tags, organic solar cells, memory devices or sensors.[4–8]

Injection or transfer molding processes to integrate conventional electronic devices into lightweight applications as well as molded interconnect (MID) devices and overmolding procedures are already well known and investigated. To name only a few composites, 3D circuits, injection molded printed wiring boards, plastic disposable biochips or micromechanical sensors and actuators can be produced with these technologies.[9–13] The integration of printed, especially inkjet printed, electronic components into lightweight materials to realize smart composite objects has barely been investigated, even though the deposition of printed electronic devices onto thin and flexible films gives the opportunity to integrate these devices easily into lightweight applications.[14,15]

We investigate an inkjet printed passive sensor for integration into lightweight structures, in our case a glass-fiber-reinforced plastic. This approach could later on be used for wireless ice detection on rotor blades. Ice accretion on rotor blades of wind turbines leads to various problems in the field of green energy. On the one hand, icing causes a shutdown of the turbines because of changed aerodynamics, and therefore a reduced yield. On the other hand, the falling down of ice fragments while the system is running brings risk to nearby humans.[16,17] Several conventional

▲ IS&T Member.

Received Mar. 11, 2016; accepted for publication May 25, 2016; published online July 1, 2016. Associate Editor: Kye-Si Kwon.

detecting systems exist, including indirect methods by observation of weather conditions, aerodynamic noise or change in the blade resonant frequency, as well as direct sensor systems, e.g., measured damping of ultrasonic waves, inductance and impedance change, temperature changes or piezoelectric sensing. The indirect methods like observation of weather conditions mostly lead to system shut downs due to assumptions independent of the actual ice accretion. Current direct sensing systems are mostly not directly deposited on the blades, which leads to low sensitivity and reliability.[16,18] Our printed sensor arrays could be directly integrated into the wind rotor blade material during its manufacture, and no wiring would be necessary. By means of the integrated passive high frequency sensor an external reading system could measure actual ice accretion. This would lead to an improvement of the reliability as well as energy yield by real-time measurements.

EXPERIMENTAL

Sensor Simulation—Printing Layout

To study the effect of ice accretion on a passive resonant structure and to investigate the behavior, electromagnetic wave simulation using the Computer Simulation Technology (CST) Microwave Studio was performed.

To simulate a two-dimensional array of resonators the unit-cell simulation model is used. It gives the opportunity to define and to model a single element which is extended to a periodic structure with virtually infinitive size by the simulation software.

The unit-cell size is 9 mm × 9 mm. The simulation model consists of three layers. The first layer is the reflector element (4.5 mm × 4.5 mm). This element's conductors are infinitely small in thickness to simplify the simulation model. The substrate is a PET foil with a thickness of 140 µm and an adhesive coating. The foil has a permittivity of 3. The third layer of the simulation model is a glass-fiber-reinforced plastic (GFRP) material with thickness of 4 mm and an assumed permittivity of 4.6. The surrounding material of the model is vacuum.

The 3D unit-cell model of one integrated sensor element in GFRP with ice accretion can be seen in Figure 1(a).

If the pattern decreased the basic reflection peak would move to a higher frequency. If the pattern increased the reflection peak would move to a lower frequency.

The square geometry was chosen because it is a simple resonant structure that enables a reflection peak depending on the dimensions of the patches and their arrangement with respect to each other. The aim was to design a resonator array where the target reflection peak occurs in the frequency range close to 24 GHz. This frequency band is license free. It is a so-called ISM band that can be used for industrial, scientific and medical applications.

In Fig. 1 (b), the first-order reflection peak of the integrated square patch shows a reflection peak in the frequency range from 15 to 17 GHz. For the sensor approach employed different materials are used. All of the materials have an influence on the occurrence of the reflection peak.

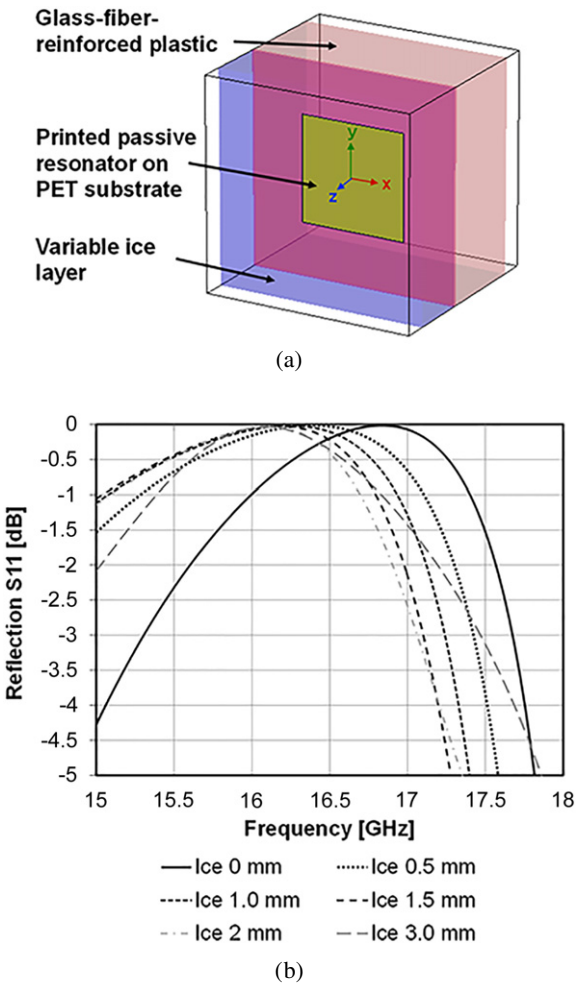

Figure 1. (a) Simulation model. (b) Simulation result showing the reflected signal power at different ice thicknesses.

From the results we can see that the 24 GHz frequency has not been achieved yet.

The results show the reflection without and with ice accretion. In the case of ice accretion, the reflection peak shifts down to lower frequencies. This is because of the permittivity of the ice, which is higher than that of the surrounding air. The higher permittivity ($\varepsilon_r = 3.175$)[19] of the ice concentrates more of the electromagnetic field inside the material, which leads to an increased capacitive load. The additional capacitive load leads to a detuning of the sensor elements, which respond with a lower resonance frequency and a shift of the reflection peak to lower frequencies.

As can be seen in Fig. 1(b), further investigations on the influence of the ice thickness need to be made. However, at this time the main objective of the research is to show that ice accretion affects the sensor behavior and causes a shift in the resonance frequency.

Out of the unit-cell simulation a 90 mm × 90 mm array was generated by the simulation software, giving the final printing layout. The pattern to be printed can be seen in Figure 2.

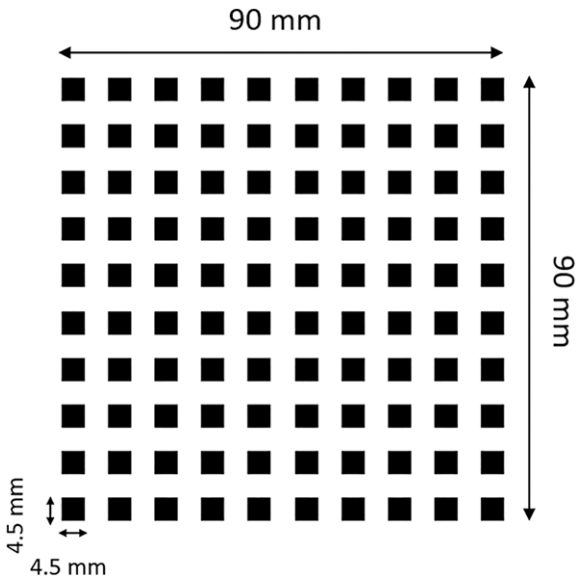

Figure 2. The printing layout—an array of squares for a passive sensing application.

Inkjet Printing

Machinery

The reflecting elements of the sensor are digitally printed by a Dimatix Materials Printer (DMP) 2831 consisting of a piezoelectric printhead with 16 nozzles. A cartridge printhead generating drops with 10 pL drop volume is used.

Materials

The printing experiments were carried out on the coated PET based substrate Novele^{TM} IJ-220 with a thickness of 140 ± 12 µm distributed by Novacentrix. This substrate was used because it is suitable for printed electronic applications. It was also chosen because of the ink performance on this substrate, namely, patterns could be printed with sharp edges and less spreading of the ink. The ink for the realization of the sensor on the substrate was the nanoparticle silver ink Silverjet DGP-40LT-15C from Advanced Nano Products. For functionality formation the ink was post-treated by infrared (IR) radiation from a short-wave twin tube emitter made of quartz glass by Heraeus (maximum specific power of 75 W/cm, 20 cm distance).

Integration

The printed array is embedded by using resin infusion technology. The material is similar to the material used in the manufacturing process of rotor blades for wind turbines. The PET substrate with the printed patterns is located on a laminating tool with the printed side on top. Then, glass-fiber-reinforced textiles (250 g/m^2) are assembled with alternate fiber directions of 0°and 90°(see Figure 3). The whole stack is covered with an additional foil and set under vacuum (up to −860 mbar). In between the foil and the laminating tool the printed foil and the glass fibers are cross-bonded in a mixture of epoxy resin and hardener by an infusion molding process. After 24 h hardening time,

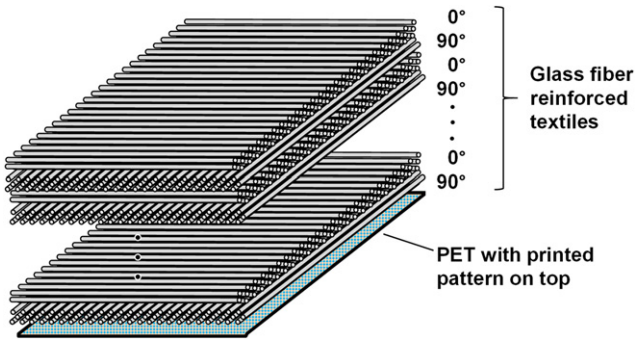

Figure 3. Layer design for the GFRP.

the glass-fiber-reinforced plastic (GFRP) composite of 4 mm thickness with the integrated printed array is finished.

The fabricated sample is the simulated model.

The performance of the sensor depends on all the different materials of the composite that surround the printed pattern. Hence, the layout of the pattern has to be adjusted to the application and to the materials used.

Analysis

Printed Pattern

First of all, the behavior of the ink on the Novele substrate was investigated. One pixel lines as well as 10 pixel lines with different drop spaces (DSs) were printed on the substrate, and the maximum DS that led to closed layers and sharp edges was found. Sharp edges and accurate dimensions are important. Open layers, blurred edges and inaccurate dimensions affect the target design of the sensor. This includes the target frequency and the quality factor of the resonance peak. Printed lines as well as squares were analyzed optically by microscopic images, morphologically by surface profile measurement (Veeco Dektak 150) and electrically by line resistance (1 px line width) as well as sheet resistance measurements (four-point Van-der-Pauw method). These measurements lead to the optimal DS to be used to realize the simulated sensor array as precisely and reliably as possible.

Reflection Performance of the Integrated Sensor

For measuring the reflection peak of the composite, two standard gain horn antennas are used in combination with a vector network analyzer (ZVA50, Rhode & Schwarz). The antennas are located in front of the sample and are arranged to perform a reflection measurement. One antenna is used to illuminate the fabricated passive sensor array while the other antenna receives the reflected signal. The vector network analyzer performs a frequency sweep to measure and analyze the reflection response in the desired frequency range from 15 to 17 GHz. From the obtained reflection response, the behavior of the passive sensor can be investigated. The measurement includes investigation of ice accretion that is generated on the composite surface to study the change in the reflection response. For this purpose, a thin ice layer was generated on the surface of the sensor device. This was done using a spray flask to produce a thin water film, and a freezer to convert it into ice. The procedure of producing

ice was applied multiple times to obtain ice layers with different thicknesses. To show the effect of ice accretion on the reflection response, several measurements—without and with ice load—were performed. Afterwards, the recorded reflection behavior was analyzed.

Because a spray flask was used for the ice layer generation, the measurement and the obtained results are difficult to reproduce due to the inhomogeneity of the ice layer. Therefore, further investigations are necessary to evaluate and reproduce the measurements.

RESULTS AND DISCUSSION

Printing

Optical Characterization

As explained above, silver lines with different DSs are printed on the Novele substrate. One pixel (px) as well as 10 px wide lines are printed. As Figure 4 shows, closed and homogeneous 1 px (top) and 10 px (bottom) lines can be realized up to DS 30 µm. In the case of 1 px lines printed with a DS higher than 30 µm, it seems that the line starts to form single drops. The effect is clearer for the 10 px lines, because there are missing areas from DS 40 µm on. Besides the increased DS, the reason for layers that are not closed might also be the coating of the Novele substrate. The coating is also verified by the stripe structure of the printed layers, which can be clearly seen in the case of the 10 px lines from DS 20 µm on.

Morphological Characterization

After the optical characterization, a profile measurement to determine the layer thickness as well as the line widths was performed. These evaluations are important to determine the DS that leads to patterns with high accuracy and optimal electrical performance for the resonator layout.

Each graph of Figures 5 and 6 represents one measurement on one line. This should only serve as an example to visualize the appearance of the lines printed with different DSs.

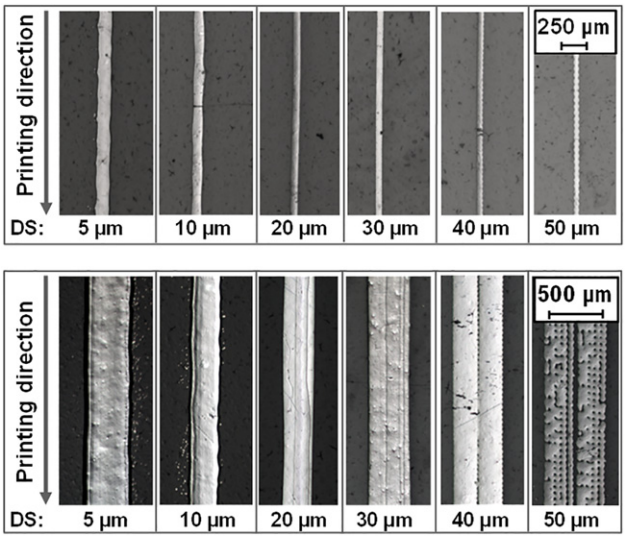

Figure 4. Silver ink on Novele PET foil printed with different DSs (top, 1 px width; bottom, 10 px width).

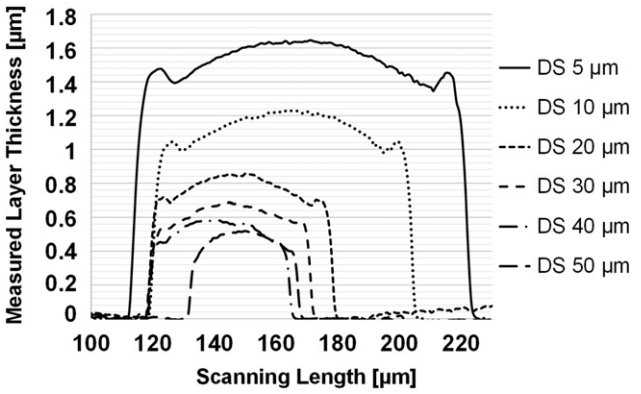

Figure 5. Dependence of layer thickness and printed line width on DS (1 px line).

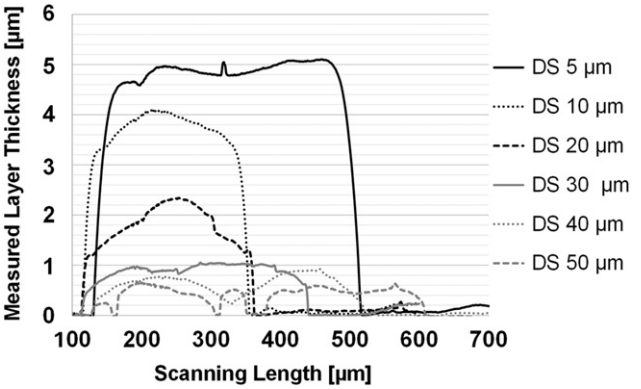

Figure 6. Dependence of layer thickness and printed line width on DS (10 px line).

Fig. 5 shows the surface profiles of the 1 px lines from DS 5 µm to 50 µm. The curves show that with increased DS the layer thickness as well as the line width decreases. It can also be seen that the lines have a higher layer thickness at the center.

The influence on the layer thickness and line width of different DSs for 10 px wide lines was also considered. In Fig. 6 it can be seen that the layer thickness rapidly decreases by increasing the DS. It is obvious that the line width increases by increasing the DS from 10 to 50 µm because of the 10 px width which was fixed digitally. The wide line printed with DS 5 µm is because a lot of material is deposited, resulting in spreading of the ink. From DS 40 µm on, the layer shows inhomogeneities until missing areas appear for DS 50 µm, which was already observed by the microscopic images. The profile measurement in general shows that the layers are not homogeneous.

The measured line widths of the 1 px lines can be seen in Figure 7.

They confirm that the printed line width decreases by increasing the DS.

The average layer thickness was also measured. Figure 8 demonstrates the average layer height of 1 px lines (left)

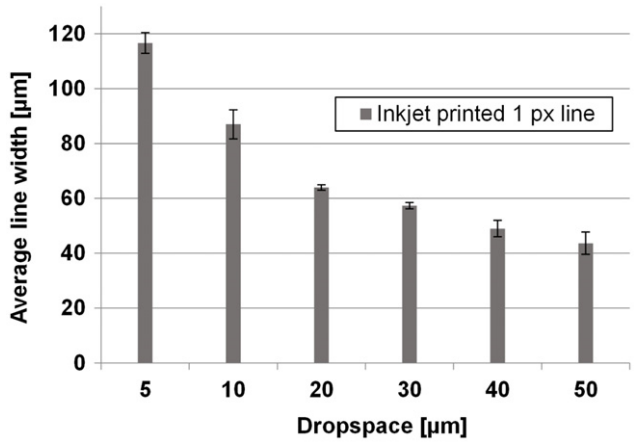

Figure 7. Average line width of 1 px line printed with different DSs.

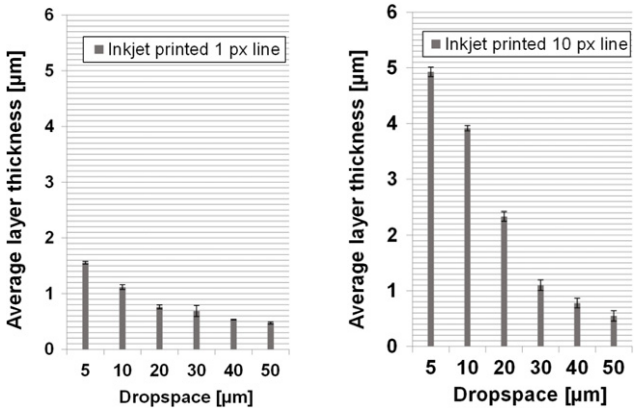

Figure 8. Average layer thickness of 1 px lines (left) and 10 px lines (right) printed with different DSs.

and 10 px lines (right) depending on different DSs. The measurement shows that the layer thickness is strongly dependent on the DS. By increasing the DS the layer height is reduced.

Electrical Characterization

Due to the fact that the printed layers have errors from DS 40 µm on, the electrical analysis was performed for DS 5, 10, 20 and 30 µm. For the line resistance, only the 1 px lines were considered, measured at a distance of 1 cm. The results can be seen in Figure 9.

The line resistances, especially for larger DSs, are very high. The reasons could be inhomogeneous layers, contacting difficulties and also, most of all, the coating of the substrate, which could lead to disturbances in the very thin lines. The smallest line resistance could be achieved with DS 5 µm ($39 \pm 4\ \Omega$), but with this DS too much material is applied and no sharp edges are possible. Additionally, thin lines could not be realized: the average line width of a 1 px line printed with DS 5 µm is 117 ± 4 µm. Moreover, the layer thickness is high compared with larger DSs (1554 ± 23 nm). It can also be seen that with larger DS the standard deviation of the measured line resistance values rapidly increases.

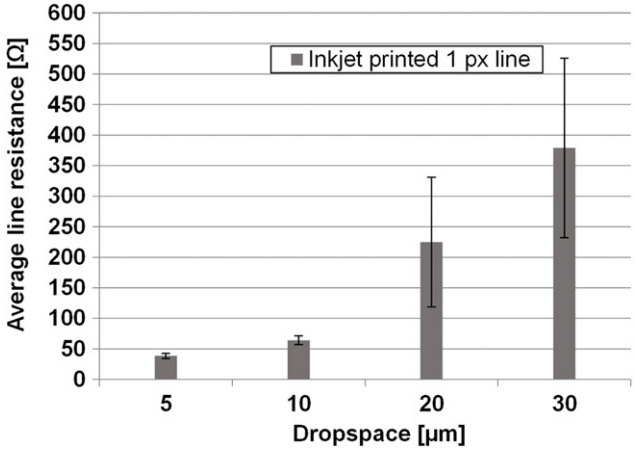

Figure 9. Average line resistance of 1 px lines printed with different DSs (measurement distance: 1 cm).

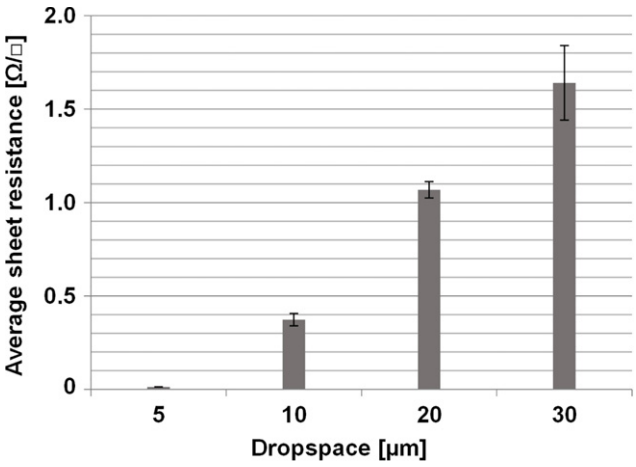

Figure 10. Average sheet resistance of 4 mm × 4 mm squares printed with different DSs.

To determine the sheet resistance of the silver ink on the particular substrate, squares of 4 mm × 4 mm are printed and measured. The sheet resistance should be as low as possible, because the sensor operates at high frequencies. A high sheet resistance means high losses, and this causes a decrease in the amplitude of the reflected signal. The aim is to provide a high quality factor that results in a high reflection amplitude. A range of sheet resistance for acceptable performance cannot be given at this early state, because the sheet resistance is not the only parameter that influences the performance of the sensor. The results are plotted in Figure 10.

As the measurements demonstrate, the sheet resistance for DS 5 µm is comparably small (~0.01 Ω/□). However, this DS will not be used for the printing of the sensor array because of the previously mentioned reasons. Regarding the sheet resistance, the values also increase by increasing the DS.

As a conclusion of the measurements and investigations made on lines and squares printed with different DSs, a final DS of 20 µm was used to print the layout of the sensor array described in the experimental part. The reasons for this are

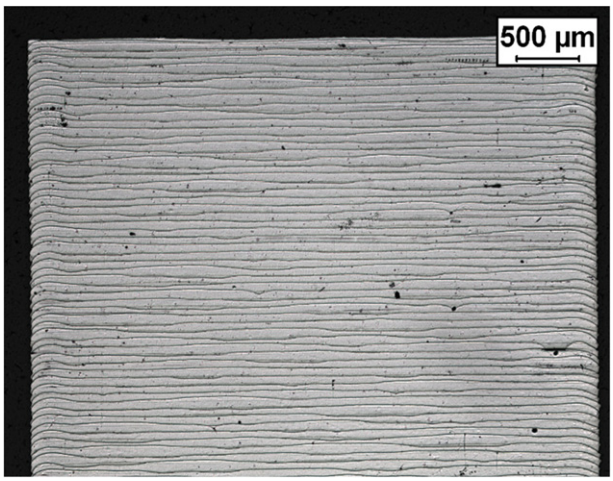

Figure 11. One sensor element printed with DS 20 µm.

to be sure to have a closed layer, sharp edges and accurate dimensions of the printed patterns. The 1 px lines printed with DS 20 µm have a line width of 64 ± 1 µm and a layer thickness of 762 ± 36 nm. The line resistance of the 1 px lines is high (225 ± 106 Ω), but if the sheet resistance is considered, the value is sufficient for the intended application ($1.07 \pm 0,04$ Ω/□).

One sensor element (4.5 mm × 4.5 mm) printed with DS 20 µm is shown as an example in Figure 11. As already mentioned, the stripe structure might result from the coating of the substrate.

Integration

The integration of the printed passive sensor on the Novele substrate by resin infusion technology into glass-fiber-reinforced plastic did not present any difficulties. The printed PET foil could be integrated without any delamination effects. The final composite can be seen in Figure 12.

Although the reflection array is encapsulated by the fabrication material, it is able to sense changes in the environment close to the senor.

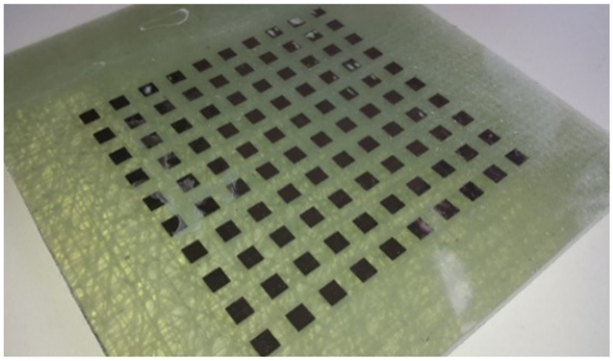

Figure 12. Composite of inkjet printed passive sensor array on coated PET foil integrated into glass-fiber-reinforced plastic.

Reflection Measurement

After the printing and integration process, the device which should be able to detect ice by passive sensing was finally characterized by its reflection behavior with and without ice load.

The reflection measurements show different reflection curves in the frequency range from 15 to 17.5 GHz. Each of the mapped reflection curves (Figure 13) is related to specific ice load and ice thickness. The approximate ice thickness was measured with a steel scale from the edge of the GFRP composite to the ice surface. However, due to inhomogeneous ice growth the value of the thickness is not completely precise, as a result of the ice growing method which is still under development. Without ice load the obtained reflection peak is around 16.6 GHz.

In the case of ice accretion and an increasing ice layer, the reflection peak moves down to lower frequencies.

In Figure 14, the diagram of frequency against ice thickness can be seen. It shows that in the case of ice accretion and an increasing ice layer, the reflection peak moves down to lower frequencies. Furthermore, the obtained results

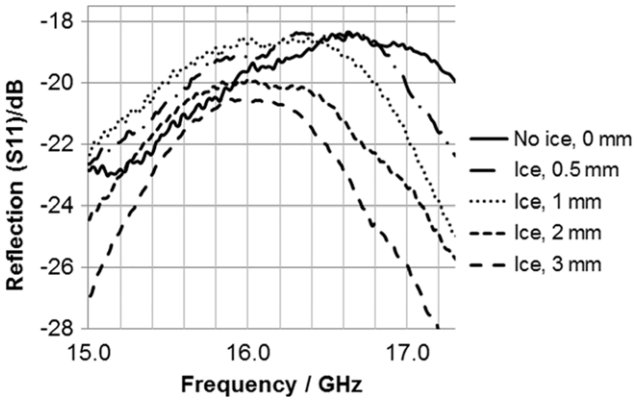

Figure 13. Results of the reflection measurement of the inkjet printed passive high frequency sensor integrated into GFRP (without ice and with different ice thicknesses).

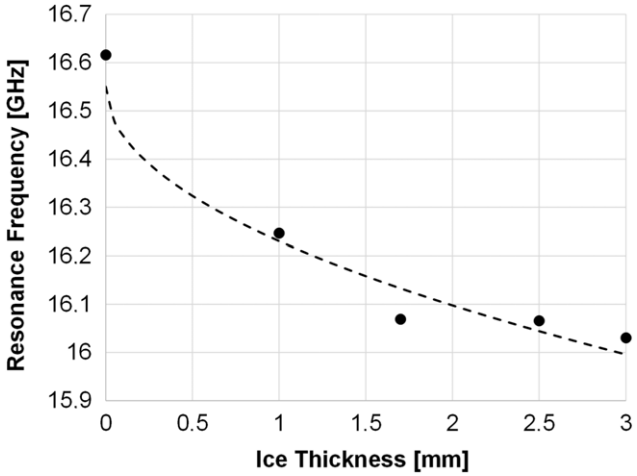

Figure 14. Shift of the reflection peak related to the ice thickness.

indicate a relation between the thickness of the ice layer and the strength of the reflection peak shift approximating to a specific value. To evaluate this assumption, further measurements and investigations as well as studies of the influence of dust and humidity are required.

In comparison to the simulation, the measurement results have a higher attenuation due to the free space loss which was not considered in the simulation.

CONCLUSION

It is demonstrated that ice detection by an inkjet printed high frequency passive sensor is possible. The sensor array printed on a coated PET foil could be successfully integrated into an epoxy resin based glass-fiber-reinforced plastic without delamination, and it was still able to sense changes in the environment.

Optimized drop spacings of the deposited silver ink on the particular substrate were demonstrated and used to realize the passive sensor array. A DS of 20 μm was found to be sufficient to realize closed and thin layers with straight dimensions. In further research, printing parameters like firing frequency, drying time and surface wettability will also have to be considered.

The reflection measurements on the printed sensor array surrounded by the GFRP showed a shift of the reflection peak to lower frequencies by ice accretion. The thickness of ice accretion depends on the location and the environmental conditions of the wind power plant. Significant ice accretion on rotor blades can reach several centimeters at the leading edge. To evaluate the assumption of the relation between the thickness of the ice layer and the strength of the shift of the reflection peak, further measurements and investigations are required in future work. Moreover, the reproducibility of the simulated ice growing on the composite has to be evaluated and performed in free space.

ACKNOWLEDGMENTS

This work was performed within the Federal Cluster of Excellence EXC 1075 "MERGE Technologies for Multifunctional Lightweight Structures" and supported by the German Research Foundation (DFG). Financial support is gratefully acknowledged.

REFERENCES

[1] A. Sridhar, T. Blaudeck, and R. R. Baumann, "Inkjet printing as a key enabling technology for printed electronics," Mater. Matters **6**, 12–15 (2011).

[2] J. Perelaer, C. E. Hendriks, A. W. M. de Laat, and U. S. Schubert, "One-step inkjet printing of conductive silver tracks on polymer substrates," Nanotechnology **20**, 165303 (2009).

[3] E. Sowade, H. Kang, K. Y. Mitra, O. J. Weiß, J. Weber, and R. R. Baumann, "Roll-to-roll infrared (IR) drying and sintering of an inkjet-printed silver nanoparticle ink within 1 second," J. Mater. Chem. C **3**, 11815 (2015).

[4] H. F. Castro, E. Sowade, J. G. Rocha, P. Alpuim, S. Lanceros-Mendez, and R. R. Baumann, "All-inkjet-printed bottom-gate thin-film transistors using UV curable dielectric for well-defined source–drain electrodes," J. Electron. Mater. **43**, 2631–2636 (2014).

[5] S. Chung, J. Jang, J. Cho, C. Lee, S. Kwon, and Y. Hong, "All-inkjet-printed organic thin-film transistors with silver gate, source/drain electrodes," Japan. J. Appl. Phys. **50**, 03CB05 (2011).

[6] R. Zichner, E. Sowade, and R. R. Baumann, "Inkjet printed WLAN antenna for an application in smartphones," Japan. J. Appl. Phys. **53**, 05HB06 (2014).

[7] J. Jung, D. Kim, J. Lim, C. Lee, and Sung Cheol Yoon, "Highly efficient inkjet-printed organic photovoltaic cells," Japan. J. Appl. Phys. **49**, 05EB03 (2010).

[8] M. Hartwig, F. Ortlepp, M. Möbius, J. Martin, T. Otto, T. Geßner, and R. R. Baumann, "Inkjet-printed quantum dot-based sensor for structural health monitoring", 2015 MRS Spring Meeting, 1788, mrss15-2135817, doi:10.1557/opl.2015.855.

[9] K. Gilleo, D. Jones, and G. Pham-Van-Diep, "Thermoplastic injection molding: new packages and 3D circuits," *ECWC 10, Conf. at IPC Printed Circuits Expo* (IPC Association Connecting Electronics Industries, Anaheim, California, 2005).

[10] M. Heckele and W. K. Schomburg, "Review on micro molding of thermoplastic polymers," J. Micromech. Microeng. **14**, R1–R14 (2004) doi:10.1088/0960-1317/14/3/R01.

[11] T. Peltola, "Integration of multilayer PWB into plastic covers by injection moulding," *Electronics System Integration Technology Conf.* (IEEE, Dresden, 2006), pp. 1342–1346, doi:10.1109/ESTC.2006.280185.

[12] D. Kashanim, V. Williams, I. V. Shvets, Y. Volkov, and D. Kelleher, "Microfluidic biochips for cell guidance and separation," *Conf. on Microtechnologies in Medicine and Biology* (IEEE, Lyon, 2000), pp. 279–282, doi:10.1109/MMB.2000.893787.

[13] E. Ehrhardt, T. Gehäußer, M. Giousouf, H. Kück, R. Mohr, and D. Warkentin, "Innovative concept for the fabrication of micromechanical sensor and actuator devices using selectively metallized polymers," Sensors Actuators A **97–98**, 473–477 (2002) doi:10.1016/S0924-4247(01)00830-5.

[14] T. Alajoki, M. Koponen, E. Juntunen, J. Petäjä, M. Heikkinen, J. Ollila, A. Sitomaniemi, T. Kosonen, J. Aikio, and J.-T. Mäkinen, "In-mold integration of electronics into mechanics and reliability of overmolded electronic and optoelectronic components," *Proc. European Microelectronics and Packaging Conf. (EMPC 09)* (IEEE, Rimini, 2009).

[15] T. Fischer, N. Wetzold, H. Elsner, L. Kroll, and A. C. Hübler, "Carbon nanotube areas—printed on textile and paper substrates," Nanomater. nanotechnol. **1**, 18–23 (2011).

[16] M. C. Homola, P. J. Nicklasson, and P. A. Sundsbø, "Ice sensors for wind turbines," Cold Reg. Sci. & Technol. **46**, 125–131 (2006).

[17] H. Seifert, A. Westerhellweg, and J. Kröning, "Risk and analysis of ice throw from wind turbines," *BOREAS 6.9* (Pyhä, Finland, 2003), 2006-01.

[18] H. Seifert, "Technical requirements for rotor blades operating in cold climate," *VI BOREAS Conf.* (Pyhatunturi, Finland, 2003).

[19] S. Fujita, T. Matsuoka, T. Ishida, K. Matsuoka, and S. Mae, "A summary of the complex dielectric permittivity of ice in the megahertz range and its applications for radar sounding of polar ice sheets," Phys. Ice Core Rec. 185–212 (2000).